JOURNAL OF MATERIALS SCIENCE 30 (1995) 3805–3810

Modelling the removal of organic vehicle from ceramic or metal mouldings: the effect of gas permeation on the incidence of defects

S. A. MATAR, M. J. EDIRISINGHE*, J. R. G. EVANS*, E. H. TWIZELL, J. H. SONG*
*Department of Mathematics and Statistics, and *Department of Materials Technology, Brunel University, Uxbridge, Middlesex, UB8 3PH, UK*

A shrinking undegraded core and a porous outer layer result, if the organic vehicle used for shaping ceramic or metal powder mouldings recedes in the interparticle space of the moulded body during pyrolysis. In the present work, a numerical model has been used which simulates the undegraded shrinking core situation and quantifies degradation of the organic vehicle and the diffusion of the resulting products in solution in the organic phase during pyrolysis of a ceramic moulding. This model is extended to include gaseous mass transport in the porous outer layer for a moulding in the shape of an infinite cylinder. The effect of resistance to gaseous mass transport in the porous outer region on defects originating in inner regions was estimated. It is shown that the greatest obstruction to mass transport is diffusion of degradation products in solution in the organic phase. However, the permeability coefficient for gas transport in the outer region begins to affect the critical heating rate required for avoidance of defects only when it is less than $10^{-15}\,m^2$.

Nomenclature

C	Concentration, $C = C(r, t)$, based on the total volume of ceramic suspension
d	Effective molecular diameter of alpha-methylstyrene
D	Diffusion coefficient, $D = D(C, T)$
e	Porosity of powder
E	Activation energy for thermal degradation
h	Remaining weight fraction of polymer
ΔH_{vap}	Enthalphy of vaporization
i	Node number
I	Pre-exponential constant in Equation 13
j	Time step
K_p	Permeability coefficient
K_0	Specific rate constant
m	Mass of monomer displaced
M	Mass of one alphamethylstyrene molecule
P	Monomer vapour pressure
P_s	Monomer vapour pressure at outer surface of the cylinder
P_1^0	Vapour pressure of monomer over its pure liquid
Q	Rate of production of monomer, based on the total volume of ceramic suspension
r	Radius of the cylinder
r_j	Distance from central axis to the inner surface of the porous layer at time step j
r_0	Initial radius of the cylinder
R	Universal gas constant
S_0	Specific surface area of powder per unit solid volume
t	Time
T	Absolute temperature
T_c	Temperature at maximum vapour pressure of monomer and at Z_c,
V	Volume of monomer
V_c	Ceramic volume fraction
V_p	Polymer volume fraction
w	Mass of monomer stored in the porous annulus
Z	Heating rate
Z_c	Critical heating rate
θ_1	Volume fraction of monomer in the polymer–monomer solution
η	Viscosity of the monomer vapour
ρ_p	Density of the polymer
χ	Polymer–monomer interaction constant

1. Introduction

The shaping of engineering ceramics by injection-moulding [1, 2] and related plastic-forming processes, such as vacuum forming, blow moulding and melt spinning [3], involves four major stages of processing. These are:

(i) dispersive mixing of the ceramic powder in an organic vehicle which permits shear or extensional flow;

(ii) shaping this mixture using plastic forming to produce the required artefacts;

0022–2461 © 1995 Chapman & Hall

(iii) removal of the organic vehicle without disrupting the arrangement of ceramic particles (in most instances by pyrolysis of the organic phase);

(iv) sintering the ceramic.

It is generally recognized that a major difficulty in these fabrication methods is stage (iii), especially when section sizes exceed about 10 mm [4]. However, it is also recognized that, if defects formed at this stage can be avoided, mass production of dimensionally accurate, complex shapes can be achieved with good process control and in this respect the possibilities offered by these manufacturing routes are far superior to other ceramic-forming methods.

Recently, there have been several attempts to develop models [5–10] which simulate removal of organic vehicle by taking into account various mass transport processes taking place in the pore architecture of a ceramic moulding during pyrolysis. These deal with liquid flow [5, 6], gaseous flow [6–8] and with diffusion of the degradation products in solution in the organic phase in the pore space [9, 10]. The last-mentioned work [10] reported an experimentally verified, numerical model which predicts the origin of defects in moulded ceramic bodies. In this model, the kinetics of thermal degradation of a polymeric vehicle, which undergoes thermal degradation to the monomer only, are combined with non-linear numerical calculations for the diffusion of degradation products in solution in the parent polymer. The concentration of monomer in an infinite cylinder is used to determine the variation of vapour pressure of monomer in the moulded body as pyrolysis proceeds, and when this exceeds ambient pressure, a bubble forms.

However, this model does not make provision for the effect on mass transport of loss of organic vehicle from the moulded body as pyrolysis proceeds and therefore underestimates the critical heating rate which can be sustained by the composite without defect formation. This has been addressed subsequently and a model which deals with the evolution of porosity in two configurations, a shrinking undegraded core and the formation of distributed porosity, has been reported elsewhere [11].

In the first case, organic vehicle recedes in the interparticle space, in preference to the formation of new internal surface. This results in a progressive decrease in the effective (organic vehicle containing) radius of the cylinder with increasing temperature. In the second case, capillary pressure throughout the porous body causes the rearrangement of residual organic vehicle in such a way that a uniform distribution of porosity is established. These modifications [11] to the earlier model [10] increased the predicted critical heating rate by a factor of 2 and 2.7 for the shrinking undegraded core and the distributed porosity situation, respectively, irrespective of cylinder radius. Real systems must lie in between these two porosity configurations depending on the mobility of the organic liquid in the pore space.

In the shrinking undegraded core situation, the concentration of monomer at the moving interface is fixed at zero and this boundary condition allows a numerical simulation for the diffusion equation to be obtained [11]. If there is resistance to flow of the gaseous degradation products through the porous outer layer, which itself increases in thickness as organic vehicle is removed, the assumption is no longer valid except at the start of pyrolysis. Therefore, in the present work, the effect of a resistance to flow in the porous outer layer was investigated.

2. Theory

The polymer is considered to degrade exclusively to monomer. Several polymers behave in this way, but polyalphamethylstyrene was used in previous work [10]. The rate of production of monomer at any temperature is given by [10]

$$\dot{Q} = \rho_p V_p K_0 \exp[-E/(RT)] \times \exp\left\{-\frac{K_0 RT^2 \exp[-E/(RT)]}{ZE} \times \left[1 - \frac{2RT}{E} + \frac{6(RT)^2}{E^2}\right]\right\} \quad (1)$$

where Z is the heating rate, E is the activation energy for thermal degradation and K_0 is the specific rate constant. The concentrations at each node can then be found by solving the non-linear differential equation

$$\frac{\partial C}{\partial t} = \frac{1}{r}\frac{\partial}{\partial r}\left(rD\frac{\partial C}{\partial r}\right) + \dot{Q} \qquad 0 < r < r_0,\ t > 0 \quad (2)$$

where the diffusion coefficient, D, is dependent on concentration and temperature and is obtained at each time step using the free volume equation for diffusion of organic molecules in polymer melts, developed by Duda *et al.* [12].

An infinite cylinder of radius, r_0, containing a ceramic volume fraction, V_c, is considered. The new polymer-containing radius, r_j, for the shrinking undegraded core model is given as a function of h_j, the remainder weight fraction of polymer at time step j (where $j = 1,2,3,...$), by [11]

$$r_j = r_0 h_j^{1/2} \quad (3)$$

At this stage, the annular region $(r_0 - r_j)$ is porous with porosity $(1 - V_c)$. The usually small shrinkage in ceramic bodies which accompanies removal of organic vehicle is ignored. Monomer vapour permeates the porous annulus and if it experiences significant resistance to flow $C(r_j, j) \neq 0$ but becomes time dependent.

This boundary condition at time step j is found from the monomer flux at time step j-1 and the permeability coefficient for the porous outer layer. At the start of pyrolysis $C(r_0, 0) = 0$ and this is a boundary condition which is used to determine the first concentration profile. For subsequent time steps $(j \geq 2)$ the mass of monomer displaced from the cylinder during the previous time step, m_{j-1}, per unit length of

cylinder, can be calculated as

m_{j-1} =

(Mass of monomer generated in time step $j-1$)

– (Mass of monomer stored in solution during time step $j-1$)

so that

$$m_{j-1} = (h_{j-2} - h_{j-1})(1 - V_c)\rho_p \pi r_0^2 - \left[\sum_{i=1}^{N} C(r_{i,j-1})\pi(r_{i+1,j-1}^2 - r_{i,j-1}^2) - \sum_{i=1}^{N} C(r_{i,j-2})\pi(r_{i+1,j-2}^2 - r_{i,j-2}^2) \right] \quad (4)$$

The rate of mass of monomer displaced per unit area for unit length of cylinder is therefore given by

$$\frac{dm}{dt} = \frac{m_{j-1}}{2\pi r_{j-1}\Delta t} \quad (5)$$

where Δt is the time step. Assuming ideal gas behaviour, the equivalent volume flux of monomer, dV/dt, at temperature T_{j-1} is given by

$$\frac{dV}{dt} = \frac{dm}{dt}\left(\frac{1}{0.1182}\frac{22.4\times10^{-3}}{273}T_{j-1}\right) \quad (6)$$

Because one mole of alphamethylstyrene (0.1182 kg) occupies $22.4\times10^{-3}\,m^3$ at STP, dV/dt (having units ms^{-1}) is the flux of alphamethylstyrene vapour emerging from the moving boundary between the undegraded core and the porous layer.

Steady-state permeation of monomer through the porous layer can be represented by a solution to the Darcy equation [13], modified to describe the situation of the present work as shown in Fig. 1. This gives

$$\frac{dV}{dt} = \frac{K_p}{\eta r_{j-1}}\frac{(P_s - P_{j-1})}{\ln(r_0/r_{j-1})} \quad (7)$$

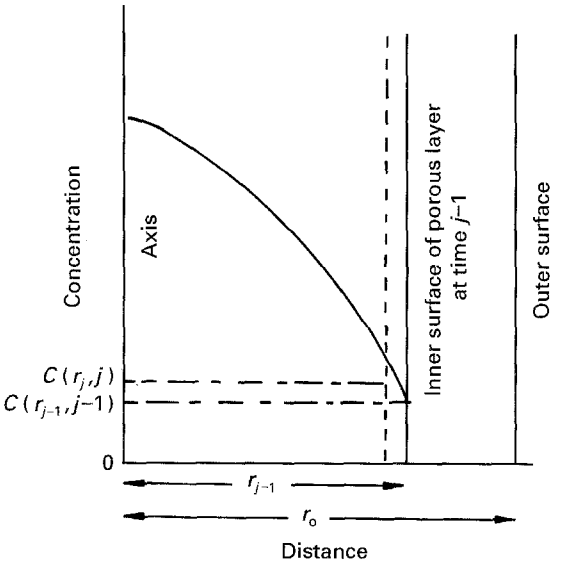

Figure 1 Schematic representation of the shrinking undegraded core model for a cylinder with an initial radius r_0.

where K_p is the permeability constant, η is the viscosity of the monomer vapour, P_s is the monomer vapour pressure at the outer surface of the cylinder where a rapid flow of gas prevails during pyrolysis. In fact, a mass transfer coefficient controls the resistance to flow at the outer surface. It depends on the gas velocity and the diffusion coefficient in the vapour phase. For the purpose of this analysis, the boundary resistance to flow is treated as negligible compared to other resistances and $P_s = 0$. P_{j-1} is the monomer vapour pressure at the inner surface of the porous layer (at $r = r_{j-1}$ in Fig. 1) and varies with time. It can be obtained at each time step by solving Equation 7 for a known flux, treating the gas as incompressible and using the K_p and η values which are evaluated as described below.

The use of Darcy's equation for gas transport through the porous layer is a simplification for several reasons:

(i) the steady state assumption is valid only for low values of Z;

(ii) viscous flow (Poiseuille flow) prevails only when the pore size is much greater than the mean free path of the diffusing molecule;

(iii) at low gas-pressure gradients or low permeability, diffusion makes a significant contribution to mass transport.

These assumptions are discussed in Section 3.

The permeability coefficient, K_p, for the alumina powder used in this work (MA2LS Alcan Chemicals, UK) has been evaluated experimentally as a function of porosity in the range 0.58–0.74 for gas flow, and satisfies the expression [14]

$$K_p = 0.99\, e^{1.39} S_V^{-2.15} \quad (8)$$

in which $S_V = V_C S_0$, where S_0 is the specific surface area of the powder per unit solid volume and e is the porosity of the powder. For MA2LS alumina, $S_0 \simeq 1191000\,m^{-1}$ and therefore, for a porosity of 50%, $K_p = 0.145\times10^{-12}\,m^2$.

The Chapman–Enskog theory [15] can be used to evaluate approximately the viscosity of alphamethylstyrene vapour using

$$\eta = \frac{5M}{16d^2}\left(\frac{RT}{\pi}\right)^{1/2} \quad (9)$$

where $M = 1.962\times10^{-25}$ kg is the mass of one molecule of alphamethylstyrene, d is the effective molecular diameter of the gas, R is the universal gas constant and T is the absolute temperature. A number of methods are available for calculating d. In the present work, the van der Waals molecular volume, V_w, using group contributions was used to calculate the equivalent diameter (assuming sphericity) of the alphamethylstyrene molecule as 6.27×10^{-10} m [16]. Substituting the values of M and d in Equation 9 gives

$$\eta_{j-1} = 1.04\times10^{-7} T_{j-1}^{1/2} \quad (10)$$

Equation 10 is used to evaluate η as a function of temperature during pyrolysis. The volume fraction of monomer, (θ_1), just beneath the moving boundary, which separates it from the porous outer layer, can be

found using the assumption that by the end of each time step, the vapour adjacent to the moving boundary is in equilibrium with its solution in the continuous phase [17]. Using the Flory–Huggins equation for activity coefficient

$$P_{j-1} = P_1^0 \theta_1 \exp[(1 - \theta_1) + \varkappa(1 - \theta_1)^2] \quad (11)$$

where θ_1 is estimated numerically at each time step j using the Newton–Raphson method with initial condition to be in the interval $0 < \theta_1 < 1$ in order to have convergence for the solution. In fact, a good approximation for θ_1 can be obtained by employing

$$\theta_1 = \frac{P_{j-1}}{3.9\ P_1^0} \quad (12)$$

because peak values of θ_1 at the critical heating rate are only a few per cent. The value of P_1^0 is found from the well-known Clausius–Clapeyron equation

$$\ln(P_1^0) = -\frac{\Delta H_{vap}}{RT} + I \quad (13)$$

In Equation 11, $\varkappa$ is the polymer–monomer interaction parameter, ΔH_{vap} and I in Equation 13 are the enthalphy of vaporization and logarithm of the pre-exponential constant, respectively.

Then

$$C(r_{j-1}, j-1) = \theta_1 \rho_p (1 - V_c) \quad (14)$$

This, together with the other boundary condition (which is valid at $r = 0$ and any time step)

$$\frac{\partial C(0,j)}{\partial r} = 0 \quad (15)$$

allows the calculation of concentration profiles at each time step j as described previously [10, 11]. The algorithm and the values used for the parameters of the degradation and diffusion equations have been listed previously [10, 11].

The procedure to be followed in making the calculations is detailed in the computing scheme shown below. The differential Equation 2 was solved using a fully implicit finite difference method [18] and the calculations were carried out using Fortran 77 on a UNIX system. LU decomposition was used to decompose the associated coefficient matrix at each time step.

2.1. Computing scheme

Input material parameters, ceramic volume fraction (0.5 was used throughout), heating rate, initial radius of cylinder and permeability coefficient.
Calculate $\dot{Q}$ at each temperature (Equation 1).
Input initial and boundary conditions.
Calculate r_j (Equation 3).
For each $j = 1$, the rest of the computing scheme is identical to that in [11].
For each time step $j = 2,3,....$
Calculate D at each concentration and temperature at time level j-1 [12].
Calculate the shrinking radius at time level j-1.
Calculate the mass of monomer m at time level j-1 (Equation 4).
Calculate the rate of mass of monomer displaced per unit length of cylinder dm/dt at time level j-1 (Equation 5).
Calculate the volume flux dV/dt at time level j-1 (Equation 6).
Calculate the viscosity of polyalphamethylstyrene, η, at time level j-1 (Equation 10).
Calculate the vapour pressure of monomer at the moving boundary at time level $j - 1$ (Equation 7).
Solve Equation 11 for θ_1, the volume fraction of monomer, using the Newton–Raphson method with starting value for θ_1, in the interval $0 < \theta_1 < 1$, to find boundary condition at time level $j - 1$ (Equation 14).
Solve for concentrations at each node at time level j (Equation 2).
Convert concentration to mole fraction based on polymer only.
Check whether monomer vapour pressure > ambient pressure (boiling criterion).
If boiling has not occurred, go to next time step.

3. Results and discussion

3.1. Critical heating rate Z_c

Table I shows Z_c values obtained for the conditions used in the present work. The values, at each cylinder radius, are equal to those given by the previous shrinking undegraded core model [11] and it is clear that taking into account permeation of gaseous degradation products through the porous outer layer for an experimentally measured value of K_p, has not affected Z_c. The temperature at which the centre vapour pressure reaches a maximum at Z_c, shown as T_c in Table I, is also the same as the previous results [11]. Taking the 5 mm diameter cylinder as an example, the data given in Fig. 2 point out the reasons for this. The maximum concentration monomer at the interface separating the porous outer layer from the core was only 3.1×10^{-2} kg m^{-3} at 294.5 °C when the core radius was 0.93 mm. This maximum concentration is extremely small, and occurs well after the centre concentration reaches a maximum ($T_c = 276$° C). Thus the earlier assumption [11] that it could be approximated to zero is justified.

Fig. 2 also shows that the change in radius of the core due to the polyalphamethylstyrene receding occurs very rapidly, in the range 260–310° C, which corresponds to the narrow degradation temperature

TABLE I Z_c and T_c values for different radii for the present work using the shrinking undegraded core model with $K_p = 0.145 \times 10^{-12}$ m^2

Cylinder radius (mm)	Z_c(K h^{-1})	T_c (°C)
0.5	111.05	332
1.0	17.04	305
1.5	5.59	292
2.0	2.52	283
2.5	1.36	276
3.0	0.82	271

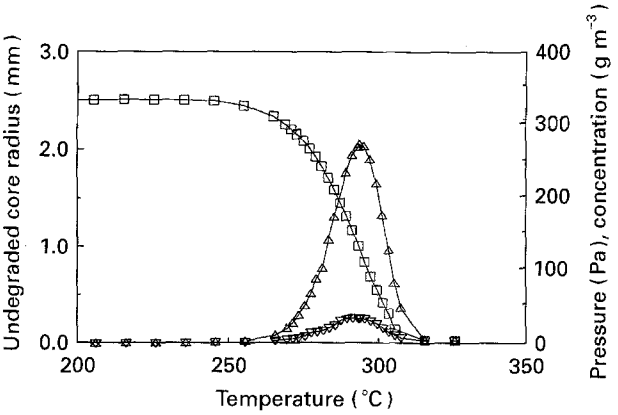

Figure 2. The variation of the (□) undegraded core radius, (△) monomer vapour pressure and (▽) monomer concentration at the moving boundary with temperature for a cylinder of 5 mm diameter at Z_c.

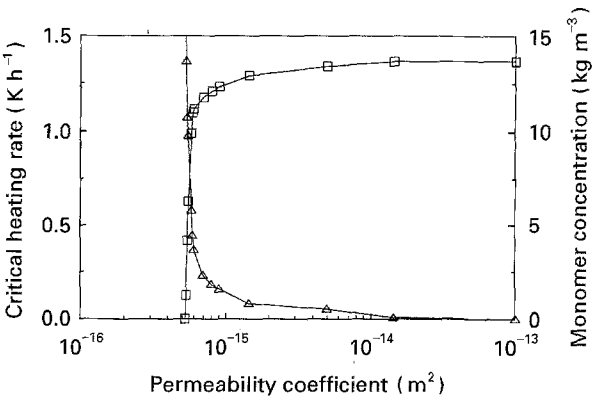

Figure 3. The effect of permeability coefficient, K_p, on (□) critical heating rate, Z_c, and (△) the monomer concentration at the moving boundary at T_c for a cyclinder of diameter 5 mm.

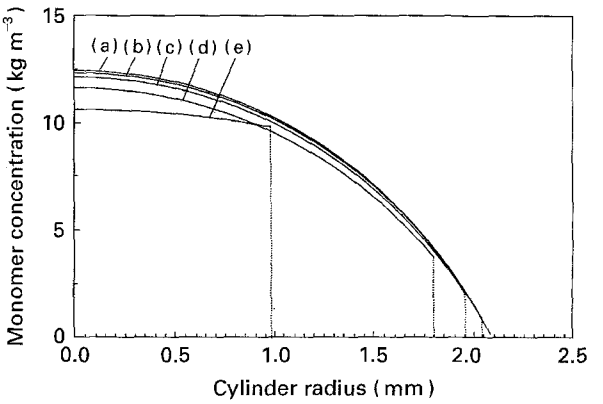

Figure 4. Effect of K_p on the concentration of monomer in the undegraded core at T_c and Z_c for a cylinder of diameter 5 mm. The dotted lines indicate the radii of the undegraded cores.
(a) $K_p = 1.45 \times 10^{-14}\,m^2$, $Z_c = 1.36\,K\,h^{-1}$ and $T_c = 549$ K.
(b) $K_p = 1.45 \times 10^{-15}\,m^2$, $Z_c = 1.29\,K\,h^{-1}$ and $T_c = 549.5$ K.
(c) $K_p = 8 \times 10^{-16}\,m^2$, $Z_c = 1.21\,K\,h^{-1}$ and $T_c = 550.5$ K.
(d) $K_p = 6 \times 10^{-16}\,m^2$, $Z_c = 1.12\,K\,h^{-1}$ and $T_c = 553$ K.
(e) $K_p = 5.5 \times 10^{-16}\,m^2$, $Z_c = 0.63\,K\,h^{-1}$ and $T_c = 558$ K.

range of this model system. It is the rapid degradation over a narrow range that partly accounts for the low values of Z_c predicted and observed [10]. The degradation temperature range moves to a lower temperature as the cylinder radius increases. This is because larger radii give rise to a lower Z_c and the degradation temperature range is sensitive to heating rate as predicted by Equation 1. Fig. 2 also shows that the monomer vapour pressure in the porous region rises to a maximum of 271 Pa at 294.5 °C.

Fig. 3 shows the effect of variation in the permeability constant. Permeability is influenced by powder-packing efficiency, particle size and size distribution and by particle shape. In this computation it was varied over several orders of magnitude. The resistance to mass transport in the porous layer began to have a significant effect on Z_c when the permeability coefficient was $< 10^{-15}\,m^2$. When it was reduced to approximately $5.3 \times 10^{-16}\,m^2$, Z_c was reduced to a very small value. Decreasing K_p below $10^{-15}\,m^2$ causes a rapid increase in monomer concentration at the moving boundary (Fig. 3) to a level comparable to that at the centre of the cylinder (e.g. curve e in Fig. 4).

Fig. 4 shows the concentration profile at T_c and Z_c for different values of K_p. The centre concentration in the cylinder is lower at lower K_p because boiling is influenced by both concentration and temperature. The caption of Fig. 4 shows that T_c increases as K_p decreases and this allows boiling to occur at a lower concentration. When the boundary condition was taken as zero, a reduction in Z_c was accompanied by a reduction in T_c according to Equation 1 and this was shown in calculated results of previous work [11]. However, when Z_c is reduced by the resistance to mass transport in the porous layer, considerably more polymer may be displaced before the centre concentration reaches a peak; as witnessed by the much smaller polymer-containing radius. This means that the temperature has progressed to a much higher value at this critical stage and this offsets the effect of reduced heating rate on the thermogravimetric loss curve predicted by Equation 1.

It is not valid to extrapolate the empirical Equation 8 much outside the range of porosity over which it was measured (58%–74%). It suggests, however, that for coarse powders such as the MA2LS alumina, it is not possible to obtain $K_p < 10^{-14}\,m^2$ because the ceramic value fraction needs to be > 0.7. Carman's modification [19] of the Kozeny equation provides an estimate of permeability of packed powder beds in terms of porosity e and volumetric specific surface area, S_0, given by

$$K_p = \frac{e^3}{5S_0^2(1-e)^2} \tag{16}$$

It should be noted that this equation has been criticized for its lack of generality [14, 20]. However, for a powder which is packed to 60% relative density ($e = 0.4$) a value of $K_p = 5.3 \times 10^{-16}$ would correspond to a specific surface area of $8.2 \times 10^6\,m^{-1}$. For monodisperse spherical particles the corresponding particle diameter would be 0.7 μm. At the effective pore diameters in such a system, the more general equation of Wakao *et al.* [21] is appropriate.

The use of Darcy's law in this context is supported by German's work [8]. However, flow behaviour in such situations can be dependent on pressure, gas

velocity and pore size. In particular, it neglects the contribution to gas transport from diffusion which is significant at low pressure gradients [22]. At low pore diameters, Knudsen flow prevails while high temperatures of intermediate pore sizes give rise to a slip–flow regime [23]. The more general expression of Wakao *et al.* [21] embraces these contributions to flow.

By neglecting the diffusion contribution to gas transport, the resistance to flow introduced by the porous region is over-estimated. Despite this, diffusion in the core has an over-riding effect on resistance to mass transport and it is to this issue that interventions to enhance the removal of organic vehicle from large section mouldings should be addressed. The maximum thickness of the porous annular region for the 5 mm diameter cylinder is 1.57 mm at the peak boundary vapour pressure at the critical heating rate (Fig. 2). If some internal porosity is developed in preference to a shrinking undegraded core, this distance will be less for a given value of h. When connected porosity develops, fast transport paths become available and the model described here will under-estimate the critical heating rate above this percolation threshold.

In deriving Equation 4 it has been assumed that the mass flow of monomer is a constant across the porous layer during a given time step. However, a mass increment, Δw, is necessary to create the pressure gradient required for viscous flow. Therefore, it is important to estimate the ratio $\Delta w/m_j$ for each time step. The mass of monomer stored in the porous annulus in each time step w is given by

$$w = \frac{4.1\times10^{-5}(1-V_c)\eta m_j}{RK_p\Delta t}[r_j^2 \ln(r_j/r_0) + 1/2(r_0^2 - r_j^2)] \quad (17)$$

Therefore

$$\frac{\Delta w}{m_j} = \frac{w_j - w_{j-1}}{m_j} \quad (18)$$

The pressure gradient used in deriving Equation 17 is calculated, neglecting the storage in the porous layer in order to avoid iteration. The maximum value $(\Delta w/m_j)$ for different values of K_p is given in Table II.

TABLE II Maximum values of $(\Delta w/m_j)$ for different permeabilities (K_p)

K_p (m^2)	$(\Delta w/m_j)_{max}$ (%)
1.45×10^{-14}	0.004
1.45×10^{-15}	0.04
5.3×10^{-16}	0.13
6×10^{-16}	0.10
8×10^{-16}	0.08

Even at very low K_p values, the $(\Delta w/m_j)_{max}$ is small and therefore the assumption is justified.

4. Conclusion

The results of a computer model which calculates the critical heating rate for ceramic mouldings suggest that the resistance to gas flow in a developing porous annulus has negligible effect on critical rate for coarse powders. This conclusion stands even when the only contribution to gas transport is viscous flow. For permeability coefficients $< 10^{-15}$ m^2 the effect of gas transport is predicted to become significant.

Acknowledgement

The authors are grateful to the Science and Engineering Research Council (SERC) for financial support under grant GR/G 04905.

References

1. M. J. EDIRISINGHE and J. R. G. EVANS, *Int. J. High Tech. Ceram.* **2** (1986) 1.
2. *Idem, ibid.* **2** (1986) 249.
3. J. R. G. EVANS, in "New Materials and their Applications", edited by D. Holland (Institute of Physics, Bristol UK, 1990) pp. 25–32.
4. J. R. G. EVANS and M. J. EDIRISINGHE, *J. Mater. Sci.* **26** (1991) 2081.
5. M. R. BARONE and J.C. ULICNY, *J. Amer. Ceram. Soc.* **73** (1990) 3323.
6. G. C. STANGLE and I.A. AKSAY, *Chem. Eng. Sci.* **45** (1990) 1719.
7. D. S. TSAI, *A. I. Ch. E. J.* **37** (1991) 547.
8. R. M. GERMAN, *Int. J. Powder Metall.* **23** (1987) 237.
9. P. CALVERT and M. CIMA, *J. Am. Ceram. Soc.* **73** (1990) 575.
10. J. R. G. EVANS, M. J. EDIRISINGHE, J. K. WRIGHT and J. CRANK, *Proc. R. Soc. Lond. A* **432** (1991) 321.
11. S. A. MATAR, M. J. EDIRISINGHE, J. R. G. EVANS and E. H. TWIZELL, *J. Mater. Res* **8** (1993) 617.
12. J. L. DUDA, J. S. VRENTAS, S. T. JU and H. T. LIU, *A. I. Ch. E. J.* **28** (1982) 279
13. A. E. SCHEIDEGGER, "The Physics of Flow High Porous Media" 3rd Edn (University of Toronto Press, 1974) pp 100–1.
14. Y. BAO and J. R. G. EVANS, *J. Eur. Ceram. Soc.* **8** (1991) 81.
15. G. A. BIRCH, "Molecular Gas Dynamics" (Clarendon Press, Oxford, 1976) pp. 73–75.
16. A. BONDI and D. J. SIMKIN, *A. I. Ch. E. J.* **6** (1960) 191.
17. R. N. MADDOX and A. L. HINES, "Mass Transfer Fundamentals and Applications" (Prentice-Hall, Englewood-Cliffs, NJ, 1985) p. 151.
18. E. H. TWIZELL, "Computational Methods for Partial Differential Equations" (Ellis Horwood, Chichester, UK, 1984) pp. 10, 11.
19. P. C. CARMAN, *J. Soc. Chem. Ind.* **57** (1938) 225.
20. J. S. REED, *J. Am. Ceram. Soc.* **76** (1993) 547.
21. N. WAKAO, S. OTANI and J. M. SMITH, *A. I. Ch. E. J.* **11** (1965) 435.
22. R. M. BARRER, in "The Solid–Gas Interface", edited by E. A. Flood, Vol. 2 (Marcel Dekker, New York, 1967) pp. 557–609
23. D. S. SCOTT and F. A. L. DULLIEN, *A. I. Ch. E. J.* **8** (1962) 113.

Received 3 November 1994
and accepted 20 January 1995